Colloids and Surfaces B: Biointerfaces 241 (2024) 114052

Contents lists available at ScienceDirect

Colloids and Surfaces B: Biointerfaces

journal homepage: www.elsevier.com/locate/colsurfb

Peptide direct growth on poly(acrylic acid)/poly(vinyl alcohol) electrospun fibers coated with branched poly(ethylenimine): A solid-phase approach for scaffolds biofunctionalization

Anna Liguori [a,1], Junwei Zhao [a,1,2], Roberto Di Gesù [a,b], Rossella De Marco [a,3], Chiara Gualandi [a,c], Natalia Calonghi [d], Antonino Pollicino [e], Luca Gentilucci [a,f,*], Maria Letizia Focarete [a,f,*]

[a] Department of Chemistry "G. Ciamician" and INSTM UdR of Bologna, University of Bologna, via Selmi 2, Bologna 40126, Italy
[b] Ri.MED Foundation, Bandiera st. 11, Palermo 90133, Italy
[c] Interdepartmental Center for Industrial Research on Advanced Applications in Mechanical Engineering and Materials Technology, CIRI-MAM, University of Bologna, Viale Risorgimento, 2, Bologna 40136, Italy
[d] Department of Pharmacy and Biotechnology, University of Bologna, via Irnerio 48, Bologna 40126, Italy
[e] Department of Civil Engineering and Architecture, University of Catania, via S. Sofia 64, Catania 95125, Italy
[f] Health Sciences & Technologies (HST) CIRI, University of Bologna, Via Tolara di Sopra 41/E, Ozzano Emilia Bologna 40064, Italy

ARTICLE INFO

Keywords:
Poly(acrylic acid)/poly(vinyl alcohol) blend
Branched poly(ethylenimine)
RGD peptides
Solid-phase synthesis
Electrospun scaffolds
Scaffold functionalization

ABSTRACT

Due to their resemblance to the fibrillar structure of the extracellular matrix, electrospun nanofibrous meshes are currently used as porous and mechanically stable scaffolds for cell culture. In this study, we propose an innovative methodology for growing peptide sequences directly onto the surface of electrospun nanofibers. To achieve this, electrospun fibers were produced from a poly(acrylic acid)/poly(vinyl alcohol) blend that was thermally crosslinked and subjected to a covalent coating of branched poly(ethylenimine). The exposed amino functionalities on the fiber surface were then used for the direct solid-phase synthesis of the RGD peptide sequence. In contrast to established strategies, mainly involving the grafting of pre-synthesized peptides onto the polymer chains before electrospinning or onto the nanofibers surface, this method allows for the concurrent synthesis and anchoring of peptides to the substrate, with potential applications in combinatorial chemistry. The incorporation of this integrin-binding motive significantly enhanced the nanofibers' ability to capture human cervical carcinoma (HeLa) cells, selected as a proof of concept to assess the functionalities of the developed material.

1. Introduction

Electrospinning represents a simple, versatile, and convenient technique for producing sub-micrometer to nanoscale fibers and fabricating nonwoven mats characterized by high specific surface area and adjustable porosity, [1–3] suitable for various applications in fields such as filtration, biotechnology, drug delivery, tissue engineering, wound dressings, biosensors, and bioseparation. [4–6] Electrospun porous mats resemble the morphology and structure of the native extracellular matrix (ECM) and are, therefore, excellent candidates as scaffolds in tissue engineering. Their ability to biomimicking the fibrillar component of the ECM, coupled with the proper selection of polymeric biomaterials depending on the type of tissues to be regenerated, allows them to reproduce the ECM functions promoting cell infiltration, morphogenesis, and regeneration. [4,7]

To further replicate the challenging complexity of biological tissues and interactions between ECM ligands and cell-surface receptors, many efforts have been focused on functionalizing electrospun scaffolds with

* Corresponding authors at: Department of Chemistry "G. Ciamician" and INSTM UdR of Bologna, University of Bologna, via Selmi 2, Bologna 40126, Italy.
E-mail addresses: luca.gentilucci@unibo.it (L. Gentilucci), marialetizia.focarete@unibo.it (M.L. Focarete).
[1] These authors contributed equally.
[2] present address: Department of Biochemistry and Molecular Medicine, University of California, Davis Medical Center Research Building I, 4635 Second Avenue Sacramento, CA 95817
[3] present address: Department of Agricultural, Food, Enviromental and Animal Sciences, University of Udine, via cotonificio 108, 33100 Udine, Italy.

https://doi.org/10.1016/j.colsurfb.2024.114052
Received 18 March 2024; Received in revised form 3 June 2024; Accepted 19 June 2024
Available online 20 June 2024

bioactive cues and enhanceing their interactions with cells. [8–12] Several strategies have been explored, including surface modification through chemical or physical methods, [13–15] immobilization of biomolecules [16,17] and cell-specific ligands, [18] coupling electrospun fibers with hydrogels to obtain composite scaffolds, [19–21] and co-electrospinning of bioactive agents with polymeric solutions. [22,23] Conjugating electrospun nanofibers with bioactive peptides targeting specific cell surface receptors, is another very powerful method to enhance material performance, and different strategies have been investigated, including coating, blending, and covalent grafting. [24,25] Two main strategies are currently utilized for the covalent binding of previously synthesized peptides. [24–29] The first approach involves grafting the peptide molecules onto the polymer chain before electrospinning. Covalent bonds between the macromolecules and the peptide, formed i.e. through a nucleophilic or radical mediated addition, [24] enable to reach an oriented and homogeneous peptide immobilization without compromising materials properties. [30] However, such an approach often leads to several drawbacks, ultimately causing the encapsulation of the bioactive segments within the polymer bulk during electrospinning, making them inaccessible. The second strategy entails immobilizing peptides onto the preformed nanofiber surface through the formation of covalent bonds, such as amide bonds, [24,26,31,32] between the functional groups of the scaffold macromolecules and the peptide moieties. This approach requires synthesizing the peptide by a traditional solid-phase protocol using polymeric resins functionalized with a suitable linker. The peptides are then obtained after cleavage from the resin support, precipitated with cold ether to remove initial impurities, and then re-grafted onto mats' fibers. Additionally, the acid treatment often required for peptide cleavage from the resin beads can potentially induce the undesired derivatization of certain amino acids, thus leading to the synthesis of incorrect peptides.

On the other hand, the direct construction of peptide libraries onto biocompatible solid supports is a less challenging and more rapid procedure, suitable for the rapid identification of cell-recognition activity, e.g. by adopting a combinatorial approach. Typically, cellulose sheets, polymer-based membranes, and glass are utilized as solid substrates. [33] Among the most intriguing examples of in-situ library synthesis, it is worth mentioning the 'one-bead-one-peptide' concept developed by Lam to support the adhesion of live human tumor cells, where a random peptide library is generated on-bead by a 'split-synthesis method'. [34,35] In another example, resins crosslinked with long PEG chains were utilized for preparing peptide libraries, for use in solid-phase library assays. [36] Xiang *et al.* prepared poly(ethylene-co-acrylic acid) thermoplastic fibers by melt-extrusion-extraction fabrication process. The fibers were reversibly dispersed for in situ synthesis of peptides HWRGWV and of peptide LXY3, and self-reassembled for binding the Fc portion of human IgG, and MDA-MB-231 breast cancer cells, respectively. [37]

The arginylglycylaspartic acid (RGD) tripeptide represents the minimal recognition motif present in many native ECM ligands of integrin receptors (e.g. fibrinogen, fibronectin, plasminogen). Integrins are heterodimeric glycoproteins acting as receptors that play a key role in cell-cell and cell-ECM interactions. [38,39] Moreover, upon activation by the respective agonists, integrins regulate various cellular functions, including adhesion, migration, invasion, proliferation, and survival/anoikis. [40] The RGD sequence has been utilized in designing RGD-conjugates involving cytotoxic drugs, diagnostic probes, nanoparticles, and nanocarriers, for applications in cancer therapy and imaging. [41–43] Additionally, RGD-functionalized bioactive surfaces have been suggested to enhance integrin-mediated cell adhesion and growth for biomedical applications, [44] particularly in diagnostics [45] and implant materials. [46] All these applications were built upon the immobilization of previously synthesized peptides onto the surface of the chosen substrates.

In this work, we propose the still unexplored direct growth of peptide sequences on the surface of electrospun nanofibers through a "grafting-from" approach, as an effective alternative to overcome the limitations of the conventional strategies. A step-by-step synthesis of a fluorescent RGD peptide was performed directly on the surface of properly designed electrospun fibers employed as solid support for peptide growth. This novel approach is expected to speed up the production of peptide-coated biocompatible fibers enabling its contextual synthesis and anchoring to the substrate, with potential application in combinatorial chemistry. The electrospun nanofibers have been skillfully designed to bear carboxyl acids functionalities, enabling the formation of a covalently linked uniform branched-poly(ethylenimine) (bPEI) coating directly on the surface of the nanofibers. The resulting mats have demonstrated their suitability as solid-phase supports for direct peptide synthesis, by anchoring the C-terminal residue to the exposed amino groups of bPEI. As a proof of concept, the ability of the resulting functionalized mats to capture human cervical carcinoma (HeLa) cells was evaluated, and the impact of the positioning of the RGD sequence within the peptide's structure on cell capture was also explored.

2. Experimental section

2.1. Materials

Poly(acrylic acid) (PAA) (M_w = 450,000 g mol^{-1}), poly(vinyl alcohol) (PVA) (M_w = 85,000–124,000 g/mol; hydrolysis degree = 87–89 %), branched-poly(ethylenimine) (bPEI) (M_w = 25,000 g/mol), ethanol, 1-ethyl-3-(3-dimethylaminopropyl)carbodiimide hydrochloride (EDCI•HCl), N-hydroxysuccinimide (NHS), dimethylformamide (DMF), methanol, dichloromethane (DCM), trifluoroacetic acid (TFA), N,N-diisopropylethylamine (DIPEA), Eosin Yellowish (EosinY), Rhodamine B (Rho), Fmoc-Gly-OH, Fmoc-Arg(Mtr)-OH, Fmoc-Asp(OtBu)-OH, Fmoc-Arg(Pbf)-OH, Fmoc-Lys(Boc)-OH, hydroxybenzotriazole (HOBt), N,N′-dicyclohexylcarbodiimide (DCC), Fmoc-Met-OH, 1,3-dimethoxybenzene, 2-(1 H-benzotriazole-1-yl)-1,1,3,3-tetramethylaminium tetrafluoroborate (TBTU) were purchased from Sigma-Aldrich, Italy. Phosphate buffer solution (PBS) was provided by Merck Co Ltd., Germany; Roswell Park Memorial Institute (RPMI) 1640 was obtained from Labtek Eurobio, Italy; Fetal Bovine Serum was purchased from Euroclone, Italy. All the chemicals were used as received. The human cervical carcinoma (HeLa) cells were obtained from ATCC.

2.2. Fabrication of crosslinked electrospun PAA/PVA mat

Electrospun mats with an estimated molar ratio between the carboxyl acid functions and the hydroxyl groups (-COOH/-OH) of 3.82 were produced from an 83:17 w/w PAA/PVA mixture. In a typical preparation procedure, 225 mg of PAA (3.13 mmol of -COOH) was solubilized in 3.5 mL of ethanol, and 46 mg (0.82 mmol of -OH) of PVA was dissolved in 1.5 mL of distilled water at 80°C. The PVA solution was added dropwise to the PAA solution, and the resulting mixture was kept under magnetic stirring for 30 min before the electrospinning process. The electrospinning was performed using an in-house electrospinning apparatus composed of a high-voltage power supply (Spellman, SL 50 P 10/CE/230), a syringe pump (KDScientific 200 series, Massachusetts, USA), a glass syringe, a stainless-steel blunt-ended needle connected with the power supply electrode, and a grounded steel plate collector (6.5 × 6.5 cm^2). The entire system was located inside a glove box (Iteco Eng., Ravenna, Italy, 100 × 75 × 100 cm^3) equipped with a temperature and humidity control system. The process was carried out at a temperature and relative humidity of 25°C and 30 %, respectively, with a solution flow rate of 20 μL min^{-1}, an applied voltage of 20 kV, and a gap of 20 cm between the needle outlet and the collector. Scaffolds with randomly arranged nanofibers were collected and labeled PAA/PVA-mats. After their production, PAA/PVA-mats were thermally crosslinked by a three-step procedure consisting of (i) thermal treatment of the mat at 140 °C for 30 min, (ii) cooling of the mat to room temperature (RT); (ii) thermal treatment of the mat at 140 °C for 1 h. The resulting

mats were labeled c-PAA/PVA-mats.

2.3. bPEI coating onto the electrospun nanofibers

62.89 mg of bPEI (0.52 mmol of -NH_2, 0.39 mmol of -NH-) was dissolved in 1 mL of DMF and stirred until complete solubilization. NHS (46.32 mg, 0.40 mmol) and EDCl•HCl (77.16 mg, 0.40 mmol) were dissolved in 2 mL of methanol and transferred into a 10 mL beaker with c-PAA/PVA-mats (52.5 mg, 0.43 mmol of free -CO_2H, 3 or 4 pieces of 2 cm×2 cm square placed in beaker vertically), and stirred for 5 min. Then, the bPEI solution was added to the beaker and shaken overnight. The reaction solution was removed from the beaker and mats were washed with DMF, water, methanol, and DCM 3 times each. For the sake of simplicity, the c-PAA/PVA mats coated with bPEI were named bPEI-mats.

2.4. Synthesis of peptides onto the nanofiber surface

2.4.1. Arg(Mtr)-Gly-Asp(OtBu)-Gly-Lys(Boc)-bPEI-mat [R(Mtr)-G-D(OtBu)-G-K(Boc)-bPEI-mat]

bPEI-mats (18 mg, 0.15 mmol of -NH_2, 0.11 mmol of -NH-) were immersed in DMF (3 mL) and the following reagents were added in sequence: Fmoc-Lys(Boc)-OH (1.6 eq, 0.41 mmol, 194 mg), NHS (1.6 eq, 0.41 mmol, 48 mg), EDCl•HCl (1.6 eq, 0.41 mmol, 79 mg). The mixture was shaken for 6 h at RT, then the solution was removed, and the mats were washed in sequence with DMF, water, methanol, and DCM (4 mL, 3 times each). The presence of unreacted amino groups was checked by the Kaiser test. Fmoc deprotection was performed by treatment of the mats with 1:4 piperidine/DMF (5 mL) for 30 min. Then the mats were washed with 5 mL of DMF. The procedure with piperidine/DMF was repeated, then the mats were washed with DMF, water, methanol, and DCM, as described above. The mats were suspended in DMF (5 mL) and Fmoc-Gly-OH (1.6 eq, 0.41 mmol, 123 mg), HOBt (1.6 eq, 0.41 mmol, 56 mg), and DCC (1.6 eq, 0.41 mmol, 85 mg) were added in sequence, and the mixture was stirred for 3 h at RT. The mats were washed with DMF, water, methanol, and DCM as described above, and the success of coupling was assessed by Kaiser test. After Fmoc deprotection as described above, Fmoc-Asp(OtBu)-OH (1.6 eq, 0.41 mmol, 170 mg), Fmoc-Gly-OH (1.6 eq, 0.41 mmol, 123 mg), and Fmoc-Arg(Mtr)-OH (1.6 eq, 0.41 mmol, 252 mg) were sequentially introduced under the same reaction conditions as described for Fmoc-Gly-OH. Finally, Fmoc was removed as usual.

2.4.2. Met-Arg(Mtr)-Gly-Asp(OtBu)-Gly-bPEI-mat [M-R(Mtr)-G-D(OtBu)-G-bPEI-mat]

bPEI-mats (25 mg, 0.21 mmol of -NH_2, 0.15 mmol of -NH-) were immersed in DMF (3 mL) and the following reagents were added in sequence: Fmoc-Gly-OH (1.6 eq, 0.58 mmol, 171 mg), NHS (1.6 eq, 0. 58 mmol, 66 mg), EDCl•HCl (1.6 eq, 0. 58 mmol, 110 mg); the mixture was shaken for 6 h at RT. Then the solution was removed, and the mats were washed 3 times in sequence with DMF, water, methanol, and DCM (3 times, 4 mL each). The presence of unreacted amino groups was checked by the Kaiser test. Fmoc deprotection was performed by treatment of the mats with 1:4 piperidine/DMF (5 mL) for 30 min, and the procedure was repeated, then the mats were washed as described above. The mats were suspended in DMF (5 mL) and Fmoc-Asp(OtBu)-OH (1.6 eq, 0. 58 mmol, 237 mg), HOBt (1.6 eq, 0. 58 mmol, 77 mg), and DCC (1.6 eq, 0. 58 mmol, 119 mg) were added in sequence, and the mixture was stirred for 3 h at RT. The mats were washed as described above, and the success of coupling was assessed by the Kaiser test. After Fmoc deprotection as described above, Fmoc-Gly-OH (1.6 eq, 0. 58 mmol, 171 mg), Fmoc-Arg(Mtr)-OH (1.6 eq, 0. 58 mmol, 350 mg), and Fmoc-Met-OH (1.6 eq, 0. 58 mmol, 213 mg) were sequentially introduced under the same reaction conditions as described for Fmoc-Asp(OtBu)-OH. Eventually, Fmoc was removed as usual.

2.4.3. H-Arg-Gly-Asp-$(Gly)_4$-Lys(EosinY)-Gly-bPEI-mat [RGD-G_4-K(EosY)-G-bPEI-mat] and H-Arg-Gly-Asp-$(Gly)_4$-Lys(Rhodamine B)-Gly-bPEI-mat [RGD-G_4-K(RhoB)-G-bPEI-mat]

General procedure. bPEI-mats (21 mg, 0.17 mmol of -NH_2, 0.13 mmol of –NH-) were immersed in DMF (5 mL) and the following reagents were added in sequence: Fmoc-Gly-OH (1.6 eq, 0. 48 mmol, 144 mg), NHS (1.6 eq, 0. 48 mmol, 56 mg), EDCl•HCl (1.6 eq, 0. 48 mmol, 93 mg), and the mixture was shaken for 6 h at RT. Then the solution was removed, and the mats were washed 3 times in sequence with DMF, water, methanol, and DCM (3 times, 4 mL each). The presence of unreacted amino groups was checked by the Kaiser test. Fmoc deprotection was done by treatment of the mats with 1:4 piperidine/DMF (5 mL) for 30 min, and the procedure was repeated, then the mats were washed as described above. The mats were suspended in DMF (5 mL) and Fmoc-Lys(Boc)-OH (1.6 eq, 0. 483 mmol, 226 mg), HOBt (1.6 eq, 0. 483 mmol, 65 mg), and DCC (1.6 eq, 0. 483 mmol, 100 mg) were added in sequence, and the mixture was stirred for 3 h at RT. The mats were washed as described above, and coupling efficacy was assessed by the Kaiser test. After Fmoc deprotection as described above, 4 Gly residues were introduced in sequence under the same reaction conditions as described for Fmoc-Lys(Boc)-OH. The resulting Fmoc-$(Gly)_4$-Lys(Boc)-Gly-bPEI-mats were then treated with 1:3 TFA/DCM (4 mL) for 1 h to remove the Boc group from side chain of Lys, and the mats were washed as described above. Either Eosin Y (1.6 eq, 0. 483 mmol, 334 mg) or rhodamine B (1.6 eq, 0. 483 mmol, 231 mg) was coupled with the free amino group of side chain of Lys in the presence of HOBt (1.6 eq, 0. 483 mmol, 65 mg), TBTU (1.6 eq, 0. 483 mmol, 155 mg), DIPEA (3.2 eq, 0. 966 mmol, 125 mg, 168 μL) for 3 h at RT. After Fmoc deprotection under the same conditions described above, the sequence was finished by coupling Fmoc-Asp(OtBu)-OH, Fmoc-Gly-OH, and Fmoc-Arg(Pbf)-OH in the presence of HOBt/DCC as described for Fmoc-Lys(Boc)-OH. The removal of Pbf and OtBu protecting groups was performed with a 5:4:1 mixture of TFA/DCM/1,3-dimethoxybenzene; the deprotection was repeated, and the peptide mats were washed as described above.

2.4.4. EosinY-$(Gly)_3$-Arg-Gly-Asp-$(Gly)_4$-bPEI-mat [EosY-G_3-RGD-G_4-bPEI-mat]) and RhodamineB-$(Gly)_3$-Arg-Gly-Asp-$(Gly)_4$-bPEI-mat [RhoB-G_3-RGD-G_4-bPEI-mat]

General procedure. bPEI-mats (20 mg, 0.16 mmol of -NH_2, 0.12 mmol of –NH-) were immersed in DMF (5 mL) and the following reagents were added in sequence: Fmoc-Gly-OH (1.6 eq, 0.459 mmol, 136 mg), NHS (1.6 eq, 0.459 mmol, 53 mg), EDCl•HCl (1.6 eq, 0.46 mmol, 88 mg); the mixture was shaken for 6 h at RT. Then the solution was removed, and the mats were washed 3 times in sequence with DMF, water, methanol, and DCM 3 times (4 mL each). The presence of unreacted amino groups was checked by the Kaiser test. Fmoc deprotection was done by treatment of the mats with 1:4 piperidine/DMF (5 mL) for 30 min, and the procedure was repeated, then the mats were washed as described above. The mats were suspended in DMF (5 mL), and all remaining Fmoc-residues (1.6 eq) were coupled in the presence of HOBt (1.6 eq, 0.46 mmol, 62 mg), and DCC (1.6 eq, 0.46 mmol, 95 mg) in DMF (5 mL). The resulting H-$(Gly)_3$-Arg(Pbf)-Gly-Asp(OtBu)-$(Gly)_4$-bPEI-mats were coupled with either Eosin Y (1.6 eq, 0.46 mmol, 318 mg) or rhodamine B (1.6 eq, 0.46 mmol, 220 mg) in the presence of HOBt (1.6 eq, 0.46 mmol, 62 mg), TBTU (1.6 eq, 0.46 mmol, 174 mg), DIPEA (3.2 eq, 0.92 mmol, 119 mg, 160 μL) for 3 h at RT. Eventually, Pbf and OtBu protecting groups were removed with a 5:4:1 mixture of TFA/DCM/1,3-dimethoxybenzene; the deprotection was repeated, and the peptide mats were washed as described above.

2.5. Determination of peptide amount

Peptide loading was calculated by spectrophotometric determination of the extent of Fmoc groups removed during the first and the last steps of the preparation of M-R(Mtr)-G-D(OtBu)-G-bPEI-mats. The procedure is briefly described herein. Fmoc-Gly-OH was coupled to the amino

groups of bPEI-mats, as reported above. After washing with DMF, water, methanol, and DCM (4 mL each, 3 times), Fmoc-Gly-bPEI-mats were treated with 5 mL of piperidine/DMF (20 %) and shaken for 30 min, then the solution was collected, and the mats were washed twice with DMF (2 mL each). The solution of piperidine in DMF was utilized to remove Fmoc and was collected with the subsequent washes. Then, 300 μL of this solution was taken out and diluted 10 times with DMF for UV–VIS measurements and the sample was analyzed with a Perkin-Elmer Lambda 45 spectrophotometer in quartz cuvettes. The Gly-bPEI-mats were utilized for prosecuting peptide synthesis, as described in the general procedure, until Fmoc-M-R(Mtr)-G-D(OtBu)-G-bPEI-mats were obtained. The last Fmoc deprotection was conducted, and the deprotection solution was collected for UV–VIS assay as described above. The amount of peptide loaded onto the mats was calculated by the formula:

$$L = \frac{A_{301} V w}{\varepsilon_c} dm$$

Where L = peptide loading in mmol gram^{-1}, A_{301} = absorbance at 301 nm, V = volume of the cleavage solution (9 mL), d = dilution factor (10), ε_c = molar extinction coefficient (7800 mL mmol^{-1}cm^{-1}), w = cuvette width (1 cm); m = sample weight.

2.6. Characterizations of the electrospun mats

Scanning electron microscopy (SEM) observations, coupled with Energy Dispersion X-ray Spectroscopy (EDS), of as-spun PAA/PVA-mats, c-PAA/PVA-mats, and bPEI-mats, before and after the peptide synthesis, were carried out using a Phenom, ProX, Thermo Fisher Scientific at an accelerating voltage of 10 kV. Morphological observations were performed on samples sputter-coated with gold. The distribution of fiber diameters was determined through the measurement of around 150 fibers using ImageJ software, and the results were given as the average diameter ± standard deviation.

Differential scanning calorimetry (DSC) was performed on as-spun PAA/PVA-mats and c-PAA/PVA-mats; PAA powder and PVA pellets were also analyzed for comparison. DSC measurements were carried out using a TA Instruments Differential Scanning Calorimeter, DSC Q100, equipped with a refrigerated cooling system (RCS). Samples were subjected to a first heating scan at 10 °C min^{-1}, a controlled cooling at 10 °C min^{-1}, and a second heating scan at 10 °C min^{-1} in N_2 atmosphere from −90 °C to 200 °C.

The chemical characterization of the as-spun PAA/PVA-mats, c-PAA/PVA-mats, and bPEI-mats was performed using a Fourier Transform Infrared Spectroscopy (ATR-FTIR) (Bruker, Alpha Model). The analysis was carried out by using FTIR microscopy in ATR mode. Each spectrum was collected in the wavenumber range 4000–400 cm^{-1}, with a resolution of 4 cm^{-1} and 64 signal accumulations.

The water stability of c-PAA/PVA-mats and bPEI-mats was investigated by measuring the gel content on 2×2 cm^2 square meshes. After their production, the mats were dried for 24 h at 40 °C under vacuum to constant weight and immersed in deionized water for 5 days at RT in a shaking bath, then a washing step of 1 h with fresh deionized water was performed. During water immersion, the sol fraction of the mats is dissolved, whereas the insoluble part (gel fraction) of each sample, retrieved from the water, was dried for 48 h at 40 °C under vacuum. The percentage gel fraction was calculated according to the equation:

$$\text{Gel fraction } (\%) = \frac{W_f}{W_i} 100$$

where W_f is the final weight of the dried sample after the removal of the sol fraction, and W_i is the initial weight of the dried samples after their production. Three replicate specimens were run for each kind of sample, and results were provided as average value ± standard deviation.

M-R(Mtr)-G-D(OtBu)-G-bPEI-mat were characterized by means of X-ray photoelectron spectroscopy (XPS). XPS spectra were recorded with a VG Microtech spectrometer with a CLAMII analyser. The X-ray source (Mg Kα, 1253.6 eV) worked at 200 kV and 10 mA at a pressure < 2 × 10^{-8} Torr. Pass energy: 100 eV for wide scans and 20 eV for narrow scans. Depth profile information was obtained by running measurements on electrons taking off from the sample surface with angles of 80°, 45° and 25°. According to the equation d= 3λ sin θ, sample depths (d) are lower when the take-off angle θ (t.o.a.) is smaller. All data analyses (linear background subtraction and peak integration) were accomplished using PeakFit software. Binding energies were referenced to the C—H level at 285.0 eV.

Confocal images were collected by means of a C1s confocal laser-scanning microscope equipped with a PlanApo oil immersion lens (Nikon, Tokyo, Japan).

2.7. In vitro cell capture experiments

Cells were grown in RPMI 1640 medium, supplemented with 10 % FCS and 2 mM L-glutamine, at 37 °C and in a 5 % CO_2 atmosphere. Prior to cell seeding, bPEI-mats and bPEI-mats coated with EosY-G_3-RGD-G_4- and RGD-G_4-K(EosY)-G- were cut into suitably sized pieces, assembled with CellCrown inserts for 24-well plates, and then sterilized using ethanol. A cell suspension of 2 × 10^5 cells/mL was added onto the top of each scaffold and incubated at 37 °C in a humidified atmosphere with 5 % CO_2. After 4 hours, the scaffolds seeded with cells were washed with phosphate buffer solution (PBS) and then fixed with methanol for 10 min at RT. The fixed cells were stained with the hematoxylin-eosin (H-E) staining kit (Abcam, Milan, Italy). The fixed cells were rinsed with distilled water for 5 min, stained with hematoxylin for 5 min, rinsed with water for 3 seconds, and stained with 5 % eosin for 3 min. After dehydration, the scaffolds were mounted and viewed under a microscope (Eclipse E400, Nikon, Tokyo, Japan). The number of cells was counted in 30 randomly selected microscopic fields. HeLa morphology on EosY-G_3-RGD-G_4-bPEI-mat and RGD-G_4-K(EosY)-G-bPEI-mat was also investigated using SEM. The observation was performed after fixing the adherent cells in 2.5 % glutaraldehyde in pH 7.4 phosphate buffer 0.01 M for 1 h and dehydrating them in a graded ethanol series. After immersion in hexamethyldisilazane, the samples were air-dried, mounted on the stub by using adhesive tape, and sputter-coated with Pd prior to the examination.

2.8. Statistical analysis

All experiments were conducted at least in triplicate on three independent samples. Data were analyzed using one-way analysis of variance (ANOVA) followed by Tukey's multiple comparison test. Group differences were considered significant if $p \leq 0.05$. Statistical analysis was carried out using GraphPad Prism software (version 5.0c, GraphPad Software, San Diego, CA, USA).

3. Results and discussion

3.1. Electrospun mats preparation

A schematic representation of the rationale behind this study is reported in Fig. 1. Electrospun fibers were fabricated using a blend of PAA and PVA, resulting in an estimated –COOH/-OH molar ratio of 3.82. The fibers were first endowed with water resistance properties by inducing the crosslinking between the –COOH and the -OH functionalities of the two polymers (PAA and PVA, respectively). Subsequently, the available carboxylic acid groups on the fiber surface were employed to covalently coat the fibers with bPEI through a condensation reaction with the amine groups of bPEI, leading to the formation of amide bonds. Lastly, the remaining unreacted amine functionalities of bPEI were utilized to initiate the synthesis of the RGD sequence directly on the surface of the fibers.

As shown in Fig. 2a, the electrospinning of the PAA/PVA blend led to

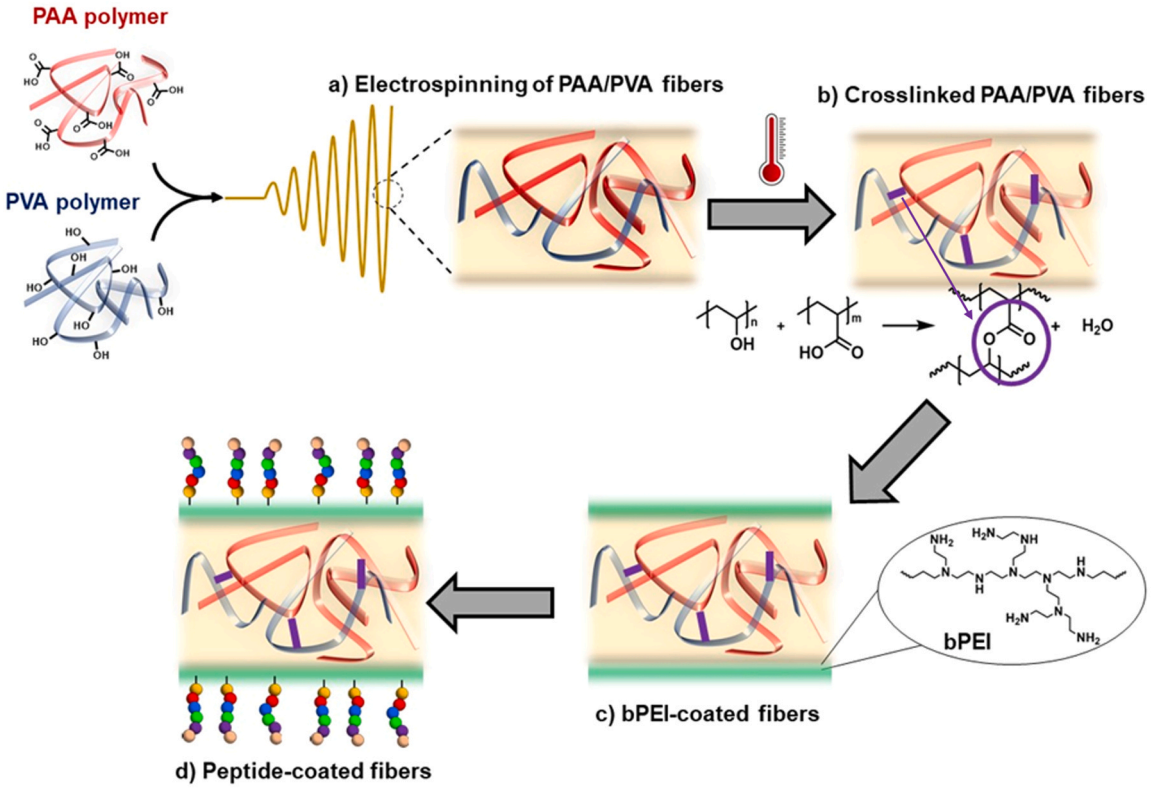

Fig. 1. Illustrative scheme of crosslinked PAA/PVA electrospun fibers coated with bPEI for the growth of peptides. The carboxylic acid groups at the fibers surface are exploited for the covalent immobilization of bPEI. Thereafter, the free amino groups of bPEI are used as linkers to connect the C-terminal amino acid of the peptides. The synthesis of the peptides occurs directly onto the electrospun mat in a solid-phase-like fashion through an iterative process.

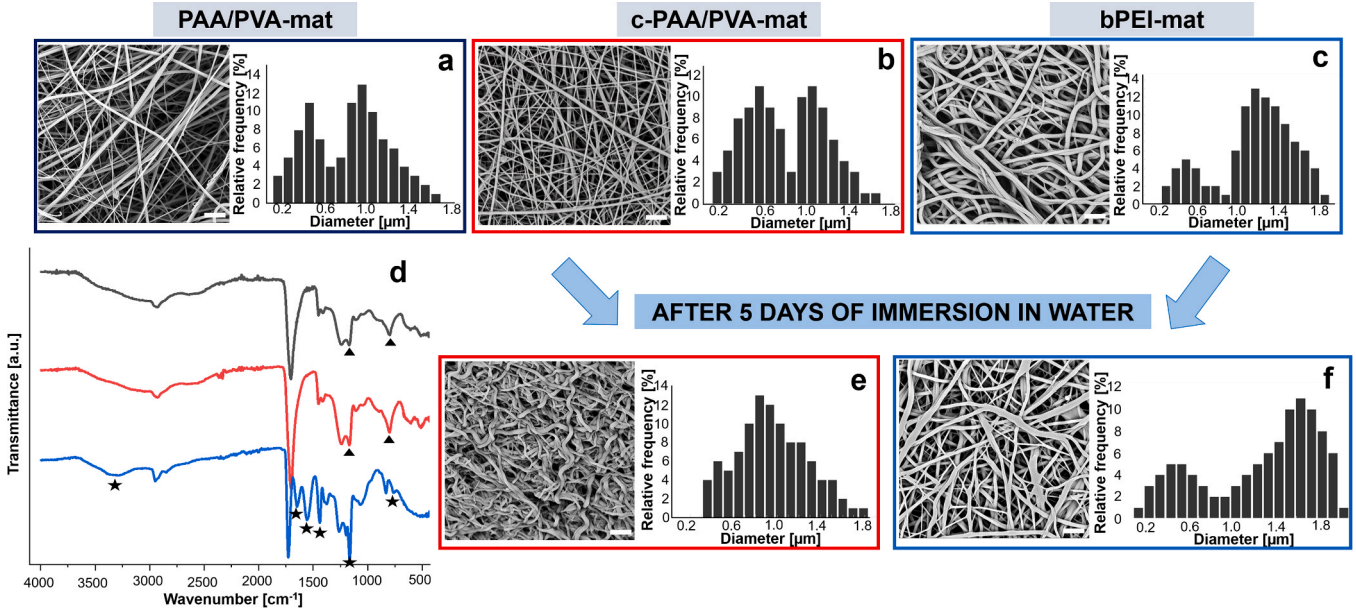

Fig. 2. SEM imaging and related fibers' diameter distributions of PAA/PVA-mat (a); c-PAA/PVA-mat (b); bPEI-mat (c); c-PAA/PVA-mat after 5 days of immersion in water (e); bPEI-mat after 5 days of immersion in water (f). Scale bar of SEM images: 5 μm. ATR-FTIR spectroscopy (d): PAA/PVA-mat (black), c-PAA/PVA-mat (red); bPEI-mat (blue). The symbol "star" indicates the bands attributed to the bPEI-mat coating; the symbol "triangle" indicates the characteristic peaks of the PAA/PVA-mat and c-PAA/PVA-mats.

regular and beads-free fibers. Comparable to the findings previously shown by Santiago-Morales *et al.*, [47] a bimodal fiber diameter distribution was observed, featuring diameters of 0.40 (±0.11) μm and 1.05 (±0.21) μm. The crosslinking procedure did not significantly alter both the morphology of the fibers and their bimodal diameter distribution (mean values were 0.52 (±0.18) μm and 1.15 (±0.18) μm) (Fig. 2b). The calorimetric characterization of PAA/PVA-mat and c-PAA/PVA-mat (Figure S1) revealed the presence of a single glass transition temperature

(T_g) value for the PAA/PVA-mat at 143 °C, in between the T_g values of the two homopolymers (157 °C and 73°C for PAA and PVA, respectively). This value closely aligns with that predicted by Fox's equation [48] (i.e. 131 °C), an empirical equation commonly used to describe the T_g-composition dependence for homogeneous polymer blends, and highlights that the two polymers are miscible within the tested composition, as previously reported. [49] After the thermal treatment, the T_g of the c-PAA/PVA-mat turned out to be hardly detectable, demonstrating the presence of a crosslinked network.

The bPEI coating procedure applied to c-PAA/PVA-mats maintained the bimodal distribution of fiber's mean diameter (Fig. 2c), characterized by values of 0.50 (±0.17) μm and 1.31 (±0.23) μm, although an overall increase in the number of the fibers exhibiting larger diameter values was observed. From the FTIR analysis of bPEI-mat (Fig. 2d), a broad band ranging from 3357 to 3295 cm^{-1}, corresponding to N-H stretching of primary and secondary amines, was detected, together with the peaks at 1650 cm^{-1} and 1550 cm^{-1} (amide I and II, respectively), 1420 cm^{-1} and 1200 cm^{-1} (amide C-N bond stretching vibration), 1050 cm^{-1} (swing vibration of $–NH_2$) and 764 cm^{-1} (out-of-plane deformation vibration of N-H) (these bands were highlighted with the symbol "star" in the Figure). Furthermore, the peaks at 846 cm^{-1} and 1239 cm^{-1} (both highlighted with the symbol "triangle" in Fig. 2d) related to C-COOH stretching and C-O stretching coupled with –OH in plane, respectively, were shifted to higher frequency after bPEI coating. The collected results confirmed the presence of amine functionalities on the surface of the bPEI-mat and the covalent linkage of the bPEI coating on the surface of the fibers through the formation of amide bonds.

The presence of the bPEI coating turned out to enhance the water stability properties of the crosslinked electrospun mats. While the as-produced mats dissolved completely upon immersion in distilled water, the c-PAA/PVA-mats exhibited a gel content of 90 (±5) %, but a partial loss of the fiber morphology and porosity was observed after 5 days of immersion (Fig. 2e). A similar value of gel content (97 (±2) %) was obtained with the introduction of the bPEI coating; however, there was a more effective retention of the fiber morphology after 5 days of immersion (Fig. 2f), also supported by the maintenance of the bimodal distributions of fiber diameter. This result can be attributed to the establishment of covalent bonds between bPEI and PAA chains, enhancing the stability of the crosslinked macromolecular network. Additionally, the reduction in available carboxylic acid groups on the fiber surface due to the bPEI coating might led to a decreased interaction between the c-PAA/PVA-mat and water. The preservation of the porosity in the bPEI-mat confirmed that the bPEI coating was successfully grafted onto the surface of the single fibers. The presence of the

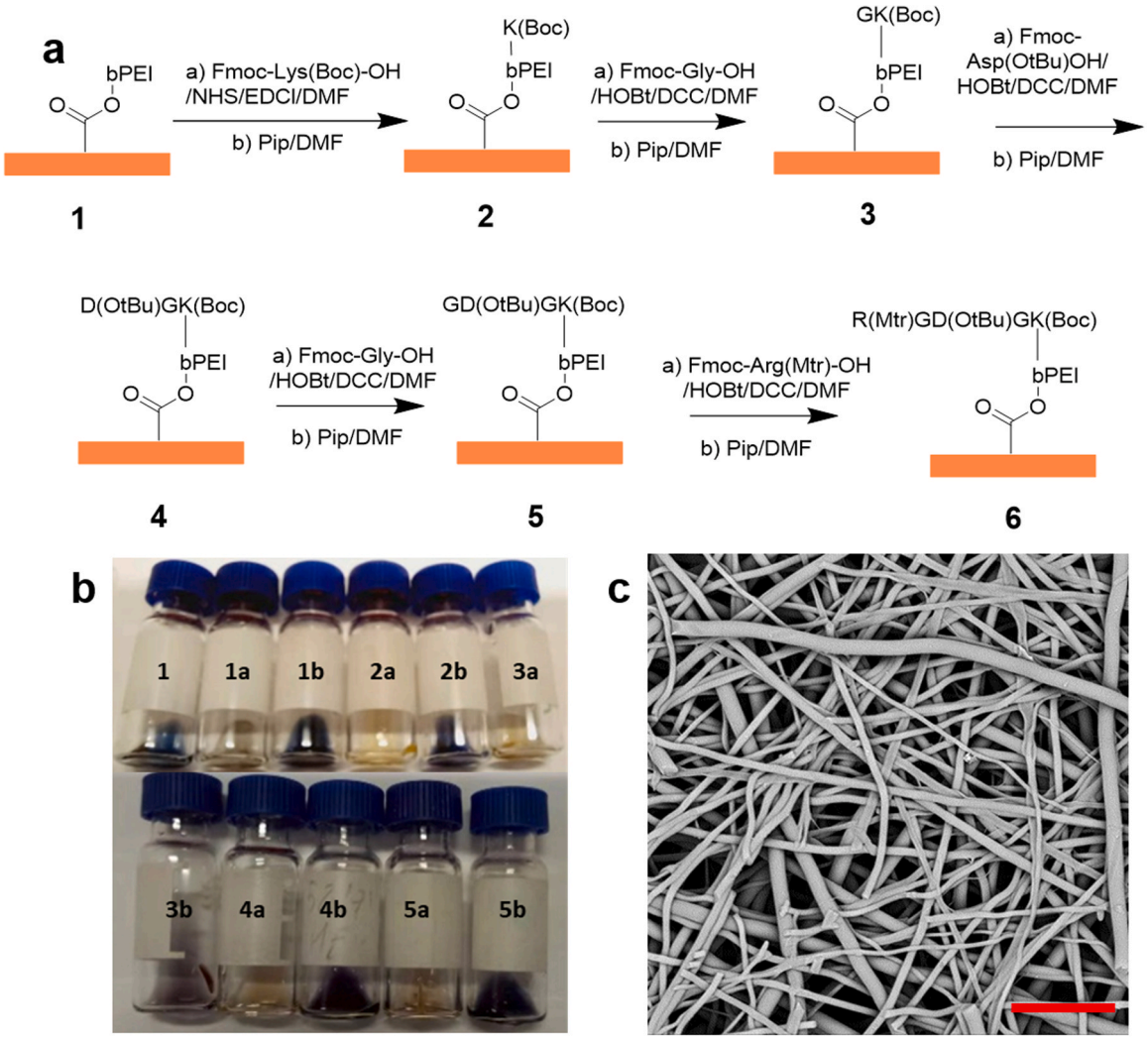

Fig. 3. (a) Schematic representation of growing R(Mtr)-G-D(OtBu)-G-K(Boc) peptide on bPEI-mats. (b) Kaiser tests for each amino acid coupling and Fmoc-deprotection: 1) bPEI-mats; 1a) coupling with Fmoc-Lys(Boc)-OH; 1b) Fmoc deprotection of Fmoc-K(Boc)-bPEI-mats; 2a) coupling with Fmoc-Gly-OH; 2b) Fmoc deprotection of Fmoc-G-K(Boc)-bPEI-mats; 3a) coupling with Fmoc-Asp(OtBu)-OH; 3b) Fmoc deprotection of Fmoc-D(OtBu)-G-K(Boc)-bPEI-mats; 4a) coupling with Fmoc-Gly-OH 4b). Fmoc deprotection of Fmoc-G-D(OtBu)-G-K(Boc)-bPEI-mats; 5a) coupling with Fmoc-Arg(Mtr)-OH; 5b) Fmoc deprotection of Fmoc-R-G-D(OtBu)-G-K(Boc)-bPEI-mats. (c) SEM image after the complete peptide growth on bPEI-mat (Scale bar: 10 μm).

coating after the immersion was verified through EDS analysis (Table S1), which demonstrated negligible reductions in nitrogen atomic concentration on coated mats after 5 days of immersion in distilled water.

3.2. Solid-phase synthesis of peptidic sequences

R(Mtr)-G-D(OtBu)-G-K(Boc)-bPEI-mat. After grafting bPEI on the fibers' surface, the peptide sequence Arg(Mtr)-Gly-Asp(OtBu)-Gly-Lys (Boc) (Fig. 3a) was grown on bPEI-mats by using HOBt and carboxydiimide as activating agents, under standard solid-phase peptide synthesis method. Glycine was introduced as a spacer, and the side chain of Lys can be used to conjugate other functional groups, such as fluorophores, small molecule diagnostic reagents, anticancer drugs, etc. The Boc protecting group of the Lysine side chain can be replaced with other protecting groups such as 1-(4,4-dimethyl-2,6-dioxycyclohex-1-ylidine) ethyl (dde), allyloxycarbonyl (alloc), so that it can be easily deprotected and grafted with other small molecules. The Kaiser test (Fig. 3b) was used to track the process of step-by-step peptide grown on bPEI-mats. The Kaiser test result of bPEI-mats showed a blue color (positive) due to the presence of bPEI free primary amino groups, while it showed a yellow color (negative) after each coupling. This result confirmed that each coupling was successfully accomplished, and the peptide was growing as expected. Furthermore, by analyzing the Fmoc content of the first amino acid and the last amino acid in the peptide grown on mats, we could confirm peptide loading (see next section).

SEM analysis performed after complete peptide growth revealed the preservation of the morphology and porosity of the mats, indicating the presence of the peptide solely on the surface of the fibers rather than within the pores of the electrospun mat (Fig. 3c).

M-R(Mtr)-G-D(OtBu)-G-bPEI-mat. The growth of M-R(Mtr)-G-D(OtBu)-G on bPEI-mats (Fig. 4a) was carried out similarly to the growth of the RGD peptide, namely by sequentially anchoring Fmoc-protected amino acids on bPEI-mats. In this procedure, we collected the 20 % solution of piperidine in DMF after the first and last deprotection reactions to quantify the content of peptide (Figs. 4b and 4c). The amount of peptide loaded onto the mats was estimated by an adaptation of a method reported in the literature, i.e. the spectrophotometrical determination of the (fluorenyl)methyl-piperidine adduct, released during Fmoc cleavage induced by the treatment with piperidine. [50] The calculated loading amount for the first amino acid was 0.607 mmol g^{-1} and for the last amino acid was 0.621 mmol g^{-1}, showing high consistency between the two measurements.

As bPEI-mats contain elements such as carbon, hydrogen, oxygen, nitrogen, XPS analysis was applied to investigate the presence of sulfur in the N-terminus of the peptide chain. Both XPS analysis and the Kaiser test confirmed that methionine constituted the last amino acid grown onto the mats, thus confirming the successful growth of the peptide.

The investigation conducted by recording a spectrum at a t.o.a. of 45° over a wide binding energy range (widescan - Fig. 5a) highlighted the presence of carbon (peak centered at ~285 eV), oxygen (peak centered at ~532 eV), nitrogen (peak centered at ~400 eV), and sulfur

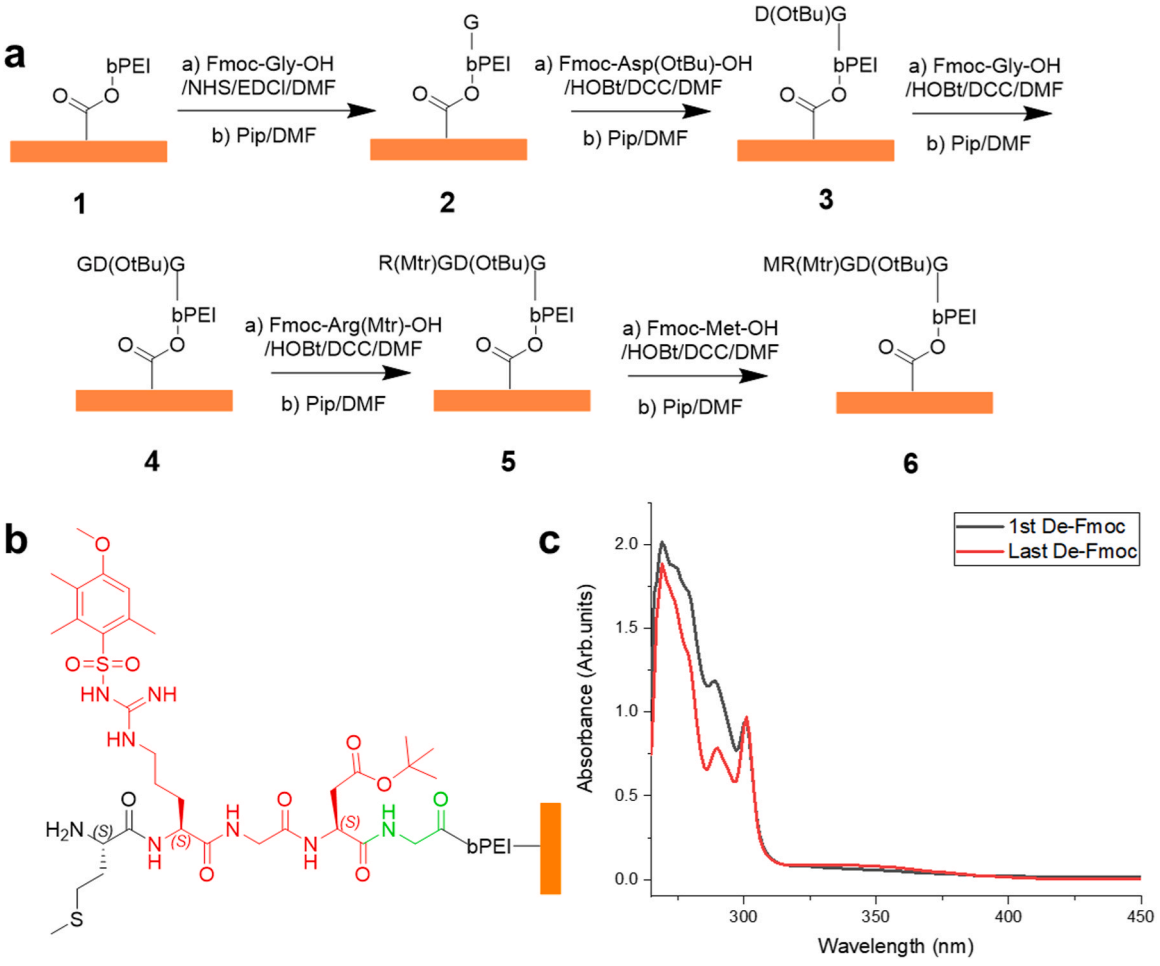

Fig. 4. (a) Schematic representation of M-R(Mtr)-G-D(OtBu)-G peptide synthesis on bPEI-mats. (b) Chemical structure of M-R(Mtr)-G-D(OtBu)-G-bPEI-mat. (c) The UV absorption spectrum of (fluorenyl)methylpiperidine in the piperidine/DMF (1/4, v/v) solution after Fmoc removal and dilution. The black line represents the UV absorption of 1-((9 H-fluoren-9-yl)methyl)piperidine solution after the first Fmoc deprotection and the red line represents the UV absorption of 1-((9 H-fluoren-9-yl) methyl)piperidine solution after the last Fmoc deprotection (De-Fmoc).

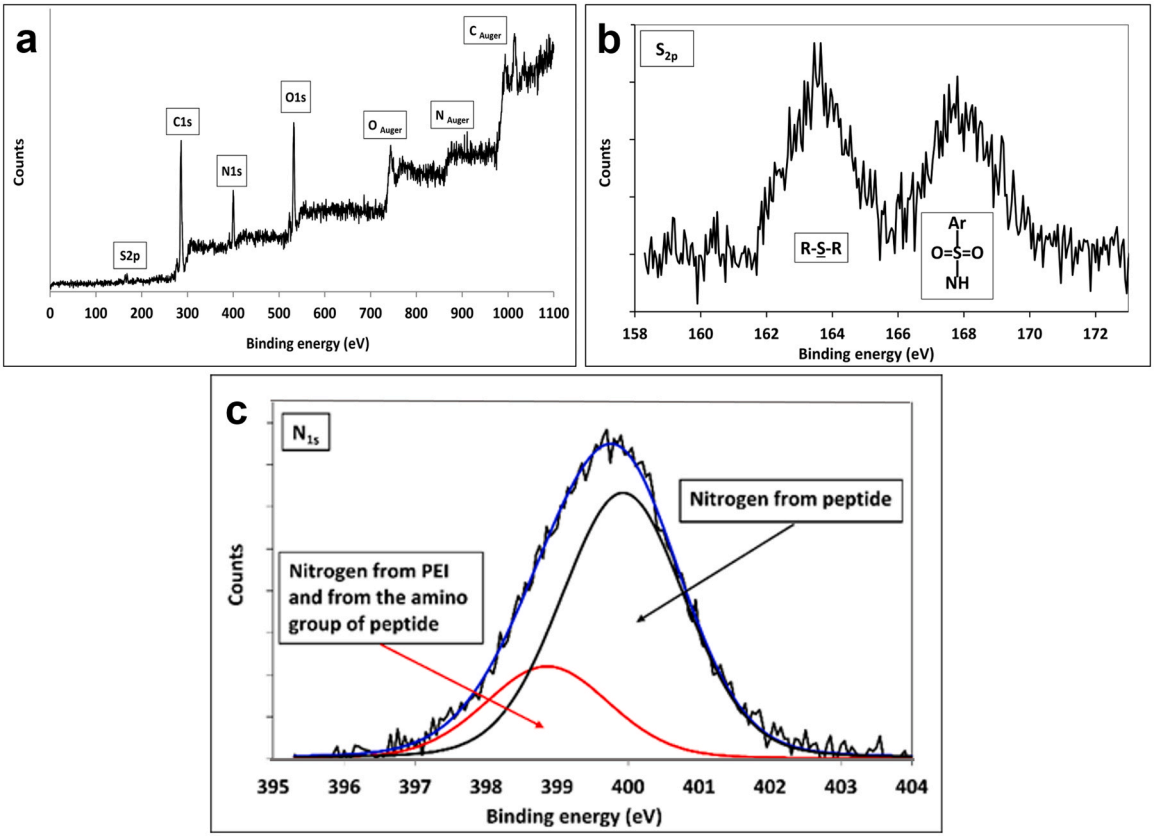

Fig. 5. XPS analysis of *M-R(Mtr)-G-D(OtBu)-G-bPEI-mat*. (a) Widescan spectrum collected at t.o.a 45°. (b) Narrowscan spectrum of S_{2p} region collected at t.o.a 45°. (c) Peak fitting of the $N_{1\,s}$ envelope collected at t.o.a 45°.

(peak centered at ~163 eV) in the outermost layers of the surface. Analyzing the signal related to sulfur atoms (Fig. 5b) confirms that they originate from the peptide. Indeed, the signal from sulfur atoms clearly consists of two peaks centered at 163.6 eV and 167.9 eV, respectively. The first peak is attributed to sulfur in thioether, while the second peak is due to sulfur involved in the sulfonic group. [45] The area under the two peaks is the same, as expected from the 1:1 ratio between sulfur atoms involved in the two organic functions. Finally, upon analyzing the $N_{1\,s}$ peak to confirm the presence of bPEI on the surface, peak fitting analysis (Fig. 5c) reveals that the nitrogen peak can be deconvoluted into two components: the first centered at 398.9 eV, clearly attributable to nitrogen atoms in bPEI and to one of the eight nitrogen atoms in the peptide (the amino one), and the second at 399.9 eV attributable to the other seven nitrogen atoms in the peptide. [51] The ratio between these two components remains 1:3 for all analyzed thicknesses. In light of the ratio between these two components of the $N_{1\,s}$ peak, it can be hypothesized that the surface contains bPEI and peptides in a molar ratio of about 6:4.

In order to assess the presence of a vertical concentration gradient of peptide on the sample surface, spectra were recorded at t.o.a. of 25, 45, and 80°. By considering the previously mentioned relationship connecting the analyzed thickness with t.o.a. and based on the inelastic mean free path (IMFP) reported by Clark for $C_{1\,s}$ electrons of 1.4 nm, information about the average compositions for thicknesses of approximately 1.8, 3.0, and 4.1 nm can be derived. [52] The results are summarized in Table 1. Observing the data in the Table, it can be concluded that there is no significant concentration gradient when moving from the outermost layers to the inner part of the sample.

RGD-G_4-K(EosY)-G-bPEI-mats, RGD-G_4-K(RhoB)-G-bPEI-mat, EosY-G_3-RGD-G_4-bPEI-mats, and RhoB-G_3-RGD-G_4-bPEI-mats. To visualize the biofunctionalization of the electrospun fibers surface by confocal microscopy, the peptide sequences were conjugated with fluorescent dyes, specifically, eosinY (EosY) or rhodamine B (RhoB). The RGD tripeptide, along with the dyes, was introduced at two alternative positions within the sequence. This design led to RGD-G_4-K(EosY)-G-bPEI-mats, RGD-G_4-K(RhoB)-G-bPEI-mats, and to EosY-G_3-RGD-G_4-bPEI-mats, RhoB-G_3-RGD-G_4-bPEI-mat, as schematically shown in Fig. 6. The confocal microscopy analysis (Fig. 6) revealed a consistent, uniform peptide coating on the fibers, and the retention of the mat's porosity, in line with the SEM analysis of Fig. 3c. No fluorescent signals were detected on the mat coated with non-fluorescent peptides, as shown in Figure S2.

Table 1
XPS mean atomic composition of M-R(Mtr)-G-D(OtBu)-G-bPEI-mat collected at thicknesses of 18, 30 e 41 Å.

Thickness [nm]	C [%]	O [%]	N [%]	S [%]
1.8	61.5 ± 2.5	23.5 ± 1.0	12.5 ± 0.5	2.5 ± 0.1
3.0	62.5 ± 1.0	22.5 ± 0.4	12.7 ± 0.2	2.3 ± 0.04
4.1	60.9 ± 0.7	23.2 ± 0.3	13.1 ± 0.2	2.8 ± 0.03

3.3. Cell adhesion experiments

To explore the impact of the RGD peptide functionalization on cancer cell adhesion, experiments were conducted by seeding human cervical carcinoma (HeLa) cells. HeLa cells are known to express high levels of RGD-binding integrins, [41] notably αvβ3, α5β1, and αvβ5. [43] The inspection of representative micrographs (Fig. 7a-c) revealed minimal adhesion on bPEI-mats lacking the RGD peptide (Fig. 7a), while noteworthy cell adhesion was evident on the RGD-functionalized mats (Fig. 7b,c). Interestingly, the most pronounced adhesion occurred on the RGD-G_4-K(EosY)-G-bPEI-mat (Fig. 7d), attributed plausibly to the more accessible positioning of the RGD sequence. As extensively documented

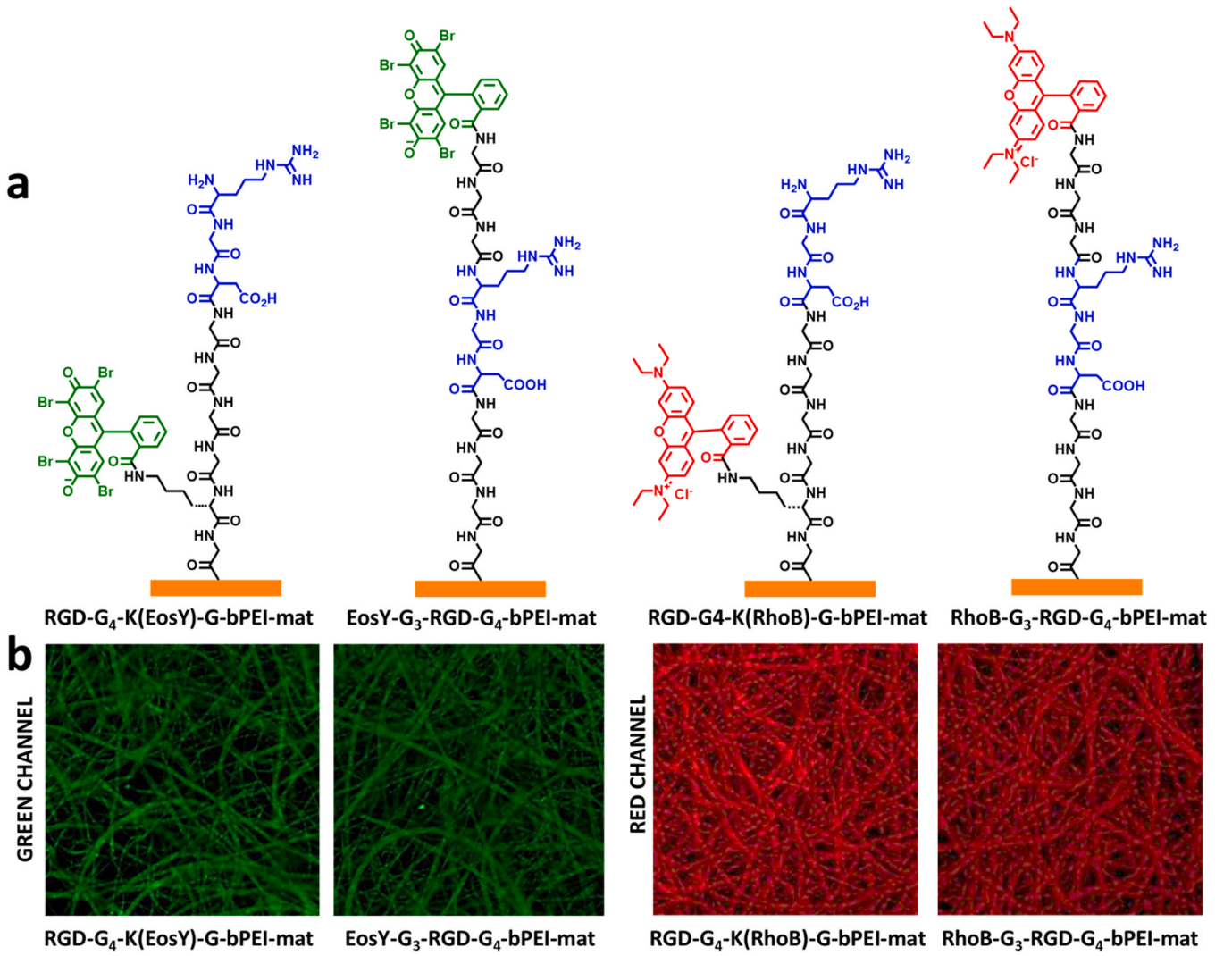

Fig. 6. (a) Structures of RGD peptides equipped with either EosY or RhoB connected by oligoGly spacers onto bPEI-mats. (b) Confocal microscope representative images collected on RGD-G_4-K(EosY)-G-bPEI-mats, EosY-G_3-RGD-G_4-bPEI-mat, RGD-G_4-K(RhoB)-G-bPEI-mats, RhoB-G_3-RGD-G_4-bPEI-mats.

in the literature, the RGD sequence is an attractive compound for enhancing cell adhesion on synthetic surfaces. [53–55]

SEM micrographs confirmed much higher cell adhesion to EosY-G_3-RGD-G_4-bPEI-mat (Fig. 7f) respect to bPEI-mat (Fig. 7e), and the highest number of adherent cells can be observed for RGD-G_4-K(EosY)-G-bPEI-mat (Fig. 7g), confirming the greater affinity of cells towards materials featuring the RGD sequence at the outermost position in the peptide sequence. Besides, while the morphology of cells adherent onto bPEI-mats was maintained (Fig. 7e), significant flattened cell morphology representative of spread cells can be observed in Fig. 7e and f. [55]

4. Conclusions

In the present work, the step-by-step synthesis of peptides directly onto the surface of properly designed electrospun fibers, is proposed for the first time. Electrospun mats of nanofibers are regarded as excellent scaffolds for testing cell adhesion. The proof of concept for this method was established using the RGD peptide. The fibrous scaffolds were obtained through electrospinning starting from a blend of PAA/PVA, followed by thermal crosslinking and subsequent bPEI coating. bPEI is often used in various applications, since it provides a large number of amino groups, rendering it useful for binding and encapsulation processes. Confirmation of the synthesis of the RGD peptide sequences was achieved through analytical techniques and XPS analysis, and the peptide content was quantified. Peptides were equipped with a fluorescent tag, therefore confocal microscopy allowed to visualize the presence of a uniform peptide coating on the fiber surface, with the fiber morphology being preserved even after the completion of all synthetic steps. The resulting materials exhibited a remarkable ability to capture HeLa cells in the presence of the RGD peptide on the fiber surface, while cell adhesion to the uncoated electrospun material was negligible.

With respect to the currently employed strategies for the immobilization of pre-synthesized peptide derivatives, the proposed approach consents to avoid tedious steps such as peptide cleavage from the resin, and re-grafting; as well as to prevent the formation of unwanted peptide derivatives generally occurring during the cleavage from the resin beads. In perspective, this proposed strategy will also enable the grafting of custom-designed peptides, including those not commercially available, and the attachment of different peptides on the same mats.

This innovative strategy holds promise for application across fibers made of different materials, functionalized with varying peptides, exploitable for biomedical applications, i.e. to enhance integrin-mediated cell adhesion and growth in diagnostics and implant materials; or as filtering materials for capturing of circulating tumor cells. This is beneficial for applications such as cancer diagnostics, where capturing circulating tumor cells from blood samples can provide valuable information for the early detection and monitoring of cancer.

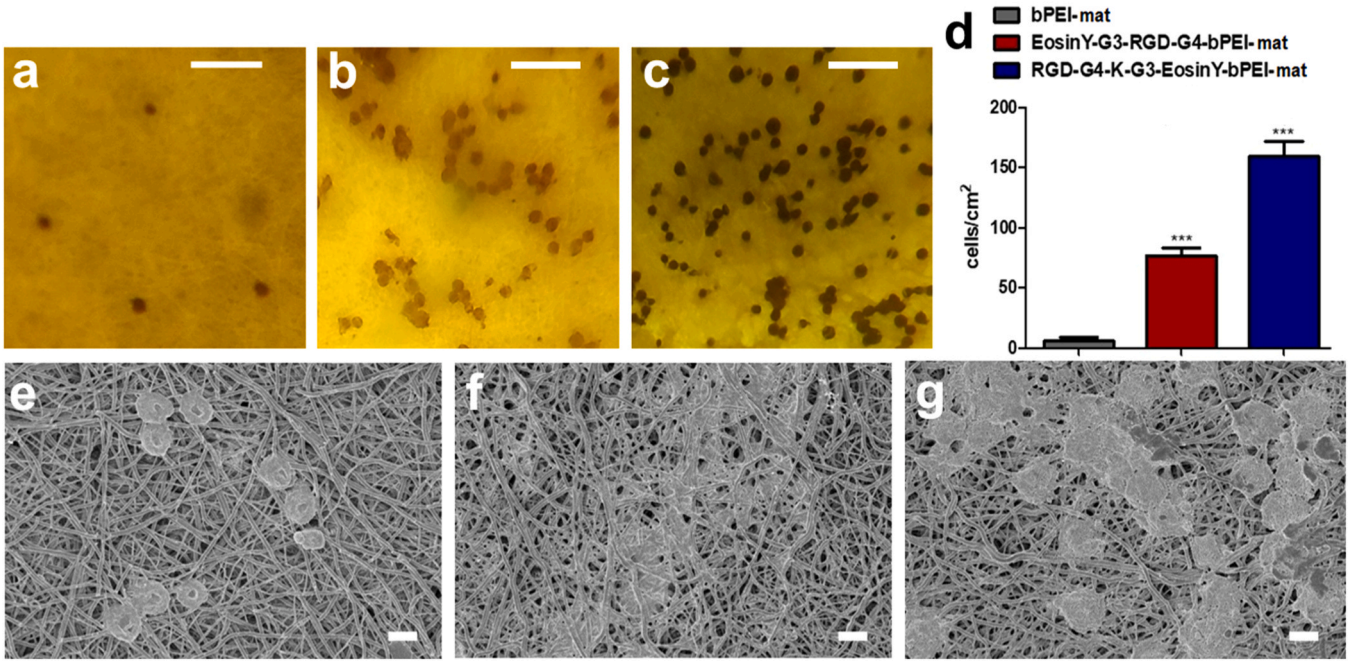

Fig. 7. Histological analyses of (a) bPEI-mat, (b) EosY-G_3-RGD-G_4-bPEI-mat, (c) RGD-G_4-K(EosY)-G-bPEI-mat, recovered from chambers after 4 h of incubation with 2×10^5 HeLa cells. Scale bar: 10 μm. (d) Number of adhered cells cm^{-2}: bars represent median values, error bars represent median absolute deviations. Statistical significance was calculated vs control. *P < 0.0001. SEM micrographs of (e) bPEI-mat, (f) EosY-G_3-RGD-G_4-bPEI-mat, and (g) RGD-G_4-K-G-EosinY-bPEI-mat, recovered from chambers after 4 h of incubation with 2×10^5 HeLa cells. Scale bar: 10 μm.

Funding

This research was funded by the Italian Ministry of University and Research (MUR), through PRIN2020 2020833Y75 and Department of Excellence Program (L. 232 01/12/2016), by the National Recovery and Resilience Plan (NRRP), Mission 04 Component 2 Investment 1.5 – NextGenerationEU, Call for tender n. 3277 dated 30/12/2021, Award Number: 0001052 dated 23/06/2022, and by Fondazione CarisBo (project #18668 "Tecnologie avanzate per il controllo e lo sviluppo di molecole innovative per la salute").

Author contributions

The manuscript was written through the contributions of all authors. All authors have given approval to the final version of the manuscript.

CRediT authorship contribution statement

Anna Liguori: Writing – review & editing, Writing – original draft, Methodology, Investigation, Formal analysis, Data curation, Conceptualization. **Junwei Zhao:** Writing – original draft, Investigation, Formal analysis, Data curation, Methodology, Conceptualization. **Roberto Di Gesù:** Writing – review & editing, Methodology, Investigation, Data curation, Conceptualization. **Rossella De Marco:** Writing – review & editing, Methodology, Investigation, Formal analysis, Data curation, Conceptualization. **Chiara Gualandi:** Writing – review & editing, Funding acquisition, Conceptualization. **Natalia Calonghi:** Writing – review & editing, Investigation, Formal analysis, Data curation. **Antonino Pollicino:** Writing – review & editing, Writing – original draft, Methodology, Investigation, Formal analysis, Data curation, Conceptualization. **Luca Gentilucci:** Writing – review & editing, Writing – original draft, Supervision, Resources, Project administration, Methodology, Data curation, Conceptualization. **Maria Letizia Focarete:** Writing – review & editing, Writing – original draft, Supervision, Resources, Project administration, Methodology, Funding acquisition, Data curation, Conceptualization.

Declaration of Competing Interest

The authors declare that they have no known competing financial interests or personal relationships that could have appeared to influence the work reported in this paper.

Data Availability

Data will be made available on request.

Acknowledgment

J.Z. thanks the China Scholarship Council for awarding a grant.

Supporting Information

Second calorimetric heating scan on PVA pellet, PAA powder, PAA/PVA mat, c-PAA/PVA mat. Energy Dispersion X-ray Spectroscopy of c-PAA/PVA mat and bPEI- mat before and after 5 days of immersion in distilled water. Confocal microscopy of bPEI-mat coated with non-fluorescent peptide.

Appendix A. Supporting information

Supplementary data associated with this article can be found in the online version at doi:10.1016/j.colsurfb.2024.114052.

References

[1] A. Greiner, J.H. Wendorff, Electrospinning: a fascinating method for the preparation of ultrathin fibers, Angew. Chem. Int. Ed. 46 (2007) 5670–5703, https://doi.org/10.1002/anie.200604646.
[2] C.T.Lim Kenry, Nanofiber technology: current status and emerging developments, Prog. Polym. Sci. 70 (2017) 1–17, https://doi.org/10.1016/j.progpolymsci.2017.03.002.
[3] A.M. Al-Dhahebi, J. Ling, S.J. Krishnan, M. Yousefzadeh, N.K. Elumalai, M.S. M. Saheed, S. Ramakrishna, R. Jose, Electrospinning research and products: the road and the way forward, Appl. Phys. Rev. 9 (2022) 011319, https://doi.org/10.1063/5.0077959.

[4] S. Agarwal, J.H. Wendorff, A. Greiner, Use of electrospinning technique for biomedical applications, Polymer 49 (2008) 5603–5621, https://doi.org/10.1016/j.polymer.2008.09.014.

[5] J. Ding, J. Zhang, J. Li, D. Li, C. Xiao, H. Xiao, H. Yang, H. Zhuang, X. Chen, Electrospun polymer biomaterials, Prog. Polym., Sci. 90 (2019) 1–34, https://doi.org/10.1016/j.progpolymsci.2019.01.002.

[6] X.L. Hu, S. Liu, G.Y. Zhou, Y.B. Huang, Z.G. Xie, X.B. Jing, Electrospinning of polymeric nanofibers for drug delivery applications, J. Controll. Release 185 (2014) 12–21, https://doi.org/10.1016/j.jconrel.2014.04.018.

[7] Y.F. Goh, I. Shakir, R. Hussain, Electrospun fibers for tissue engineering, drug delivery, and wound dressing, J. Mater. Sci. 48 (2013) 3027–3054, https://doi.org/10.1007/s10853-013-7145-8.

[8] F. Karimi, A.J. O'Connor, G.G. Qiao, D.E.Heath Integrin, clustering matters: a review of biomaterials functionalized with multivalent integrin-binding ligands to improve cell adhesion, migration, differentiation, angiogenesis, and biomedical device integration, Adv. Healthc. Mater. 7 (2018) 1701324, https://doi.org/10.1002/adhm.201701324.

[9] X. Xiea, Y. Chen, X. Wang, X. Xu, Y. Shen, A.R. Khan, A. Aldalbahi, E.F. Allison, G. L. Bowlin, M. El-Newehy, X. Mo, Electrospinning nanofiber scaffolds for soft and hard tissue regeneration, J. Mater. Sci. Technol. 59 (2020) 243–261, https://doi.org/10.1016/j.jmst.2020.04.037.

[10] M.B. Taskin, T. Ahmad, L. Wistlich, L. Meinel, M. Schmitz, A. Rossi, J. Groll, Bioactive electrospun fibers: fabrication strategies and a critical review of surface-sensitive characterization and quantification, Chem. Rev. 121 (2021) 11194–11237, https://doi.org/10.1021/acs.chemrev.0c00816.

[11] S. Politi, F. Carotenuto, A. Rinaldi, P. Di Nardo, V. Manzari, M.C. Albertini, R. Araneo, S. Ramakrishna, L. Teodori. Smart ECM-based electrospun biomaterials for skeletal muscle regeneration. Nanomaterials 10 (2020) 1781, DOI10.3390/nano10091781.

[12] H.S. Yoo, T.G. Kim, T.G. Park, Surface-functionalized electrospun nanofibers for tissue engineering and drug delivery, Adv. Drug Deliv. Rev. 61 (2009) 1033–1042, https://doi.org/10.1016/j.addr.2009.07.007.

[13] S. Khaliliazar, S. Akbari, M.H. Kish, Modification of poly(L-lactic acid) electrospun fibers and films with poly(propylene imine) dendrimer, Appl. Surf. Sci. 363 (2016) 593–603, https://doi.org/10.1016/j.apsusc.2015.12.070.

[14] L.S. Dolci, A. Liguori, A. Merlettini, L. Calza, M. Castellucci, M. Gherardi, V. Colombo, M.L. Focarete, Antibody immobilization on poly(L-lactic acid) nanofibers advantageously carried out by means of a non-equilibrium atmospheric plasma process, J. Phys. D Appl. Phys. 49 (2016) 274003, https://doi.org/10.1088/0022-3727/49/27/274003.

[15] L.S. Dolci, S.D. Quiroga, M. Gherardi, R. Laurita, A. Liguori, P. Sanibondi, A. Fiorani, L. Calzà, V. Colombo, M.L. Focarete, Carboxyl surface functionalization of poly(L-lactic acid) electrospun nanofibers through atmospheric non-thermal plasma affects fibroblast morphology, Plasma Process. Polym. 11 (2014) 203–213, https://doi.org/10.1002/ppap.201300104.

[16] B. Niemczyk-Soczynska, A. Gradys, P. Sajkiewicz, Hydrophilic surface functionalization of electrospun nanofibrous scaffolds in tissue engineering, Polymers 12 (2020) 11, https://doi.org/10.3390/polym12112636.

[17] S. Smith, K. Goodge, M. Delaney, A. Struzyk, N. Tansey, M. Frey, A Comprehensive review of the covalent immobilization of biomolecules onto electrospun nanofibers (DOI), Nanomaterials 11 (2020) 11, https://doi.org/10.3390/nano10112142.

[18] P.L. Benitez, S. Mascharak, A.C. Proctor, S.C. Heilshorn, Use of protein-engineered fabrics to identify design rules for integrin ligand clustering in biomaterials, Integr. Biol. 8 (50) (2016) 50–61, https://doi.org/10.1039/c5ib00258c.

[19] Q. Fu, C. Duan, Z. Yan, Y. Li, Y. Si, L. Liu, J. Yu, B. Ding, Nanofiber-based hydrogels: controllable synthesis and multifunctional applications, Macromol. Rapid Commun. 39 (2018) 1800058, https://doi.org/10.1002/marc.201800058.

[20] A. Liguori, M.E. Gino, S. Panzavolta, P. Torricelli, M. Maglio, A. Parrilli, C. Gualandi, C. Griffoni, G. Barbanti Brodano, M. Fini, M.L. Focarete, Tantalum nanoparticles enhance the osteoinductivity of multiscale composites based on poly (lactide-co-glycolide) electrospun fibers embedded in a gelatin hydrogel, Mater. Today Chem. (2022) 100804, https://doi.org/10.1016/j.mtchem.2022.100804.

[21] A. Liguori, A. De Vita, G. Rossi, L.S. Dolci, S. Panzavolta, C. Gualandi, L. Mercatali, T. Ibrahim, M.L. Focarete, A modular composite device of poly(ethylene oxide)/poly(butylene terephthalate) (PEOT/PBT) nanofibers and gelatin as a dual drug delivery system for local therapy of soft tissue tumors, Int. J. Mol. Sci. 23 (2022) 3239, https://doi.org/10.3390/ijms23063239.

[22] L. Liverani, A. Liguori, P. Zezza, C. Gualandi, M. Toselli, A.R. Boccaccini, M. L. Focarete, Nanocomposite electrospun fibers of poly(ε-caprolactone)/bioactive glass with shape memory properties, Bioact. Mater. 11 (2022) 230–239, https://doi.org/10.1016/j.bioactmat.2021.09.020.

[23] E. Norris, C. Ramos-Rivera, G. Poologasundarampillai, J.P. Clark, Q. Ju, A. Obata, J.V. Hanna, T. Kasuga, C.A. Mitchell, G. Jell, J.R. Jones, Electrospinning 3D bioactive glasses for wound healing (DOI), Biomed. Mater. 15 (1) (2020) 015014, https://doi.org/10.1088/1748-605X/ab591d.

[24] R. Bucci, F. Vaghi, E. Erba, A. Romanelli, M.L. Gelmi, F. Clerici, Peptide grafting strategies before and after electrospinning of nanofibers, Acta Biomater. 122 (2021) 82–100, https://doi.org/10.1016/j.actbio.2020.11.051.

[25] M. Shafiq, S.H. Kim, Covalent immobilization of MSC-affinity peptide on poly(L-lactide-co- ε-caprolactone) copolymer to enhance stem cell adhesion and retention for tissue engineering applications, Macromol. Res. 24 (2016) 986–994, https://doi.org/10.1007/s13233-016-4138-x.

[26] T.G. Kim, T.G. Park, Biomimicking extracellular matrix: cell adhesive RGD peptide modified electrospun poly(D,L-lactic-co-glycolic acid) nanofiber mesh, Tissue Eng. 12 (2006) 221–233, https://doi.org/10.1089/ten.2006.12.221.

[27] A. Yıldız, A.A. Kara, F. Acartürk, Peptide-protein based nanofibers in pharmaceutical and biomedical applications, Int. J. Biol. Macromol. 148 (2020) 1084–1097, https://doi.org/10.1016/j.ijbiomac.2019.12.275.

[28] T.H. Zhu, K. Yu, M.A. Bhutto, X.R. Guo, W. Shen, J. Wang, W.M. Chen, H. El-Hamshary, S.S. Al-Deyab, X.M. Mo, Synthesis of RGD-peptide modified polyester-urethane urea electrospun nanofibers as a potential application for vascular tissue engineering, Chem. Eng. J. 315 (2017) 177–190, https://doi.org/10.1016/j.cej.2016.12.134.

[29] X. Gao, X.H. Zhang, J.L. Song, X. Xu, A.X. Xu, M.K. Wang, B.W. Xie, E.Y. Huang, F. Deng, S.C. Wei, Osteoinductive peptide-functionalized nanofibers with highly ordered structure as biomimetic scaffolds for bone tissue engineering, Int. J. Nanomed. 10 (2015) 7109–7128, https://doi.org/10.2147/IJN.S94045.

[30] J. Yu, A.R. Lee, W.H. Lin, C.W. Lin, Y.K. Wu, W.B. Tsai, Electrospun PLGA fibers incorporated with functionalized biomolecules for cardiac tissue engineering, Tissue Eng. Part A 20 (2014) 13–14, https://doi.org/10.1089/ten.tea.2013.0008.

[31] H. Sun, S. Onneby, Facile polyester surface functionalization via hydrolysis and cell-recognizing peptide attachment, Polym. Int. 55 (2006) 1336–1340, https://doi.org/10.1002/pi.2090.

[32] T.G. Kim, T.G. Park, Surface functionalized electrospun biodegradable nanofibers for immobilization of bioactive molecules, Biotechnol. Prog. 22 (2006) 1108–1113, https://doi.org/10.1021/bp060039t.

[33] K.S. Lam, M. Renil, From combinatorial chemistry to chemical microarray, Curr. Opin. Chem. Biol. 6 (2002) 353–358, https://doi.org/10.1016/S1367-5931(02)00326-5.

[34] K.S. Lam, S.E. Salmon, E.M. Hersh, V. Hruby, W.M. Kazmierski, R.J. Knapp, A new type of synthetic peptide library for identifying ligand-binding activity, Nature 354 (1991) 82–84, https://doi.org/10.1038/354082a0.

[35] K.S. Lam, M. Lebl, V. Krchnak, The "one-bead-one-compound" combinatorial library method, Chem. Rev. 97 (1997) 411–448, https://doi.org/10.1021/cr9600114.

[36] M. Renil, M. Ferreras, J.M. Delaisse, N.T. Foged, M. MeldalPEGA supports for combinatorial peptide synthesis and solid-phase enzymatic library assays. J Pept Sci. 4 (1998) 195-210, https://doi.org/10.1002/(SICI)1099-1387(199805)4:33.0.CO;2-R.

[37] B. Xiang, G. Sun, K.S. Lam, K. Xiao, Novel poly(ethylene-co-acrylic acid) nanofibrous biomaterials for peptide synthesis and biomedical applications, J. Biomed. Mat. Res. 95A (2010) 245–255, https://doi.org/10.1002/jbm.a.32819.

[38] R.O. Hynes, Integrins: versatility, modulation, and signaling in cell adhesion, Cell 69 (1992) 11–25.

[39] M.S. Maginnis, J.C. Forrest, S.A. Kopecky-Bromberg, S.K. Dickeson, S.A. Santoro, M.M. Zutter, G.R. Nemerow, J.M. Bergelson, T.S. Dermody, T.S. Beta1, integrin mediates internalization of mammalian reovirus, J. Virol.. 80 (2006) 2760–2770, https://doi.org/10.1128/JVI.80.6.2760-2770.2006.

[40] F.G. Giancotti, E. Ruoslahti, Integrin signaling (doi:), Science 285 (1999) 1028–1033, https://doi.org/10.1126/science.285.5430.1028.

[41] M. Anselmi, A. Borbly, E. Figueras, C. Michalek, I. Kemker, L. Gentilucci, N. Sewald. Linker hydrophilicity modulates the anticancer activity of RGD–cryptophycin conjugates, Chem. Eur. J. 27 (2021) 1015–1022, https://doi.org/10.1002/chem.202003471.

[42] J. Zhao, F. Santino, D. Giacomini, L. Gentilucci, Integrin-targeting peptides for the design of functional cell-responsive biomaterials, Biomedicines 8 (2020) 307, https://doi.org/10.3390/biomedicines8090307.

[43] F. Danhier, A. Le Breton, V. Préat, RGD-based strategies to target αvβ3 integrin in cancer therapy and diagnosis, Mol. Pharm. 9 (2012) 2961–2973.

[44] M. Kantlehner, D. Finsinger, J. Meyer, P. Schaffner, A. Jonczyk, B. Diefenbach, B. Nies, H. Kessler, Selective RGD mediated adhesion of osteoblasts at surfaces of implants, Angew. Chem., Int. Ed. 38 (1999) 560–562.

[45] A. Greco, L. Maggini, L. De Cola, R. De Marco, L. Gentilucci, Diagnostic implementation of fast and selective integrin-mediated adhesion of cancer cells on functionalized Zeolite L monolayers, Bioconjugate Chem. 26 (2015) 1873–1878, https://doi.org/10.1021/acs.bioconjchem.5b00350.

[46] C. Mas-Moruno, R. Fraioli, F. Rechenmacher, S. Neubauer, T.G. Kapp, H. Kessler, alfavbeta3- or alfa5beta1-Integrin-selective peptidomimetics for surface coating, Angew. Chem. Int. Ed. 55 (2016) 7048–7067, https://doi.org/10.1002/anie.201509782.

[47] J. Santiago-Morales, G. Amariei, P. Letón, R. Rosal, Antimicrobial activity of poly (vinyl alcohol)-poly(acrylic acid) electrospun nanofibers, Colloids Surf. B 146 (2016) 144–151, https://doi.org/10.1016/j.colsurfb.2016.04.052.

[48] T.G. Fox, Influence of diluent and of copolymer composition on the glass temperature of a polymer system, Bull. Am. Phys. Soc. 1 (1956) 123.

[49] H. Vázquez-Torres, J.V. Cauich-Rodríguez, C.A. Cruz-Ramos, Poly(vinyl alcohol)/poly(acrylic acid) blends: Miscibility studies by DSC and characterization of their thermally induced hydrogels, J. Appl. Polym. Sci. 50 (1993) 777–792, https://doi.org/10.1002/app.1993.070500505.

[50] M. Gude, J. Ryf, P.D. White, An accurate method for the quantitation of Fmoc-derivatized solid phase supports, Lett. Pept. Sci. 9 (2002) 203–206.

[51] G. Beamson, D. Briggs, High-Resolution XPS of Organic Polymers. The Scienta ESCA 3000 Database, Wiley, Chichester, 1992.

[52] D.T. Clark, H.R. Thomas, Application of ESCA to polymer chemistry. XVI. Electron Mean Free Paths as a function of kinetic energy in polymeric films determined by means of ESCA, J. Polym. Sci.: Polym. Chem. Ed. 15 (1977) 2843–2867.

[53] S. Drotleff, U. Lungwitz, M. Breuniga, A. Dennis, T. Blunk, J. Tessmar, A. Gopferich, Biomimetic polymers in pharmaceutical and biomedical sciences,

Eur. J. Pharm. Biopharm. 58 (2004) 385–407, https://doi.org/10.1016/j.ejpb.2004.03.018.

[54] R.G. Le Baron, K.A. Athanasiou, Extracellular matrix cell adhesion peptides: functional applications in orthopedic materials, Tissue Eng. 6 (2000) 85–103, https://doi.org/10.1089/107632700320720.

[55] S.P. Massia, J.A. Hubbell, An RGD spacing of 440 nm is sufficient for integrin alphaVbeta 3-mediated fibroblast spreading and 140 nm for focal contact and stress fiber formation, J. Cell Bio 114 (1991) 1089–1100, https://doi.org/10.1083/jcb.114.5.1089.